


Time-domain buffeting response prediction of a long-span bridge: A hybrid machine learning framework

Foad Mohajeri Nav, Reda Snaiki^{*} 

Department of Construction Engineering, École de Technologie Supérieure, Université du Québec, Montréal, QC, H3C 1K3 Canada

ARTICLE INFO

Keywords:

Long-span bridges
Buffeting response
Machine learning
Dimensionality reduction

ABSTRACT

As bridge spans continue to increase, wind-induced vibrations become a major concern for structural integrity and serviceability. Buffeting, caused by the impinging turbulence, significantly impacts fatigue life and serviceability of long-span bridges. Consequently, accurate and rapid assessment of buffeting-induced responses is crucial for various applications, including real-time monitoring and risk assessment. This study introduces a novel hybrid machine learning framework designed to simulate the buffeting-induced response of long-span bridges over time, addressing key limitations in existing approaches. Unlike previous studies, which often focused on localized predictions, limited wind scenarios, frequency-domain analysis, and suffered from error accumulation over time, the proposed framework captures the complete time-history response across multiple degrees of freedom, providing a more comprehensive understanding of the bridge's dynamic behavior. The framework combines autoencoders and Long Short-Term Memory (LSTM) networks to enhance the efficiency and accuracy of time-series prediction. Initially, autoencoder networks compress the high-dimensional wind speed and bridge displacement data into lower-dimensional latent spaces, capturing essential features while reducing computational cost. Subsequently, an LSTM network leverages these compressed representations to model temporal dependencies within the buffeting response, predicting the bridge's response based on encoded wind speed. The final predictive model integrates both autoencoders and the trained LSTM: the first autoencoder encodes raw wind speed, the LSTM predicts the latent bridge response from this encoding, and the second autoencoder reconstructs the final predicted bridge response vector. The model's effectiveness is evaluated through a simplified representation of the Lysefjord Bridge, rigorously assessing both interpolation and extrapolation performances. The proposed model achieves a good simulation accuracy on both training and testing sets, making it a compact and computationally efficient tool for real-time monitoring and assessment of bridges under various wind conditions.

1. Introduction

Long-span bridges present a unique engineering challenge due to their inherent flexibility and susceptibility to wind-induced vibrations. Buffeting, which results from the interaction between turbulent wind fields and the bridge, is one of the most commonly observed wind-induced forces [1–5]. Continuous buffeting can lead to localized structural fatigue, impacting the bridge's lifespan and serviceability [6]. Therefore, there is an increasing demand for precise computational modeling and prediction of the buffeting response of bridges.

The determination of the buffeting-induced response can be typically achieved using three major approaches, namely wind tunnel experiments, numerical simulations, and field measurements. While wind

tunnel testing remains a cornerstone technique [7–10], due to its ability to characterize the aerodynamic characteristics, estimate key parameters, and assess stability, several limitations can arise with this approach. For example, it is significantly challenging to accurately replicate the complex on-site wind turbulence in a controlled environment. In addition, the significant expense and time associated with model construction and testing can limit its application for existing bridges. On the other hand, numerical simulations have gained more popularity due to their outstanding performances in predicting the bridge buffeting responses. They typically involve two techniques, namely computational fluid dynamics (CFD) [11], which simulate the complex wind flow around the bridge structure and provide the aerodynamic loads on the bridge, and computational structural dynamics (CSD) which model the

^{*} Corresponding author.

E-mail address: reda.snaiki@etsmtl.ca (R. Snaiki).

<https://doi.org/10.1016/j.istruc.2025.108286>

Received 17 July 2024; Received in revised form 27 November 2024; Accepted 19 January 2025

Available online 28 January 2025

2352-0124/© 2025 The Author(s). Published by Elsevier Ltd on behalf of Institution of Structural Engineers. This is an open access article under the CC BY-NC-ND license (<http://creativecommons.org/licenses/by-nc-nd/4.0/>).

structural response of the bridge due to the aerodynamic loads [12]. While traditionally applied in a decoupled manner, recent efforts focus on fluid-structure interaction (FSI) coupling, where CFD and CSD simulations are dynamically linked to capture the intricate interplay between wind and structure [13]. However, the computational power required for accurate simulations remains a significant hurdle. This constraint impedes the application of numerical simulations in probabilistic and risk assessment, and near-real-time predictions. Field measurements offer the most direct and accurate assessment of bridge buffeting response as they capture the actual behavior under natural wind excitation [14]. This method has been instrumental in validating and refining analytical and numerical models, providing valuable insights into buffeting characteristics for bridges like the Tsing Ma suspension bridge [15], Runyang suspension bridge [16], Sutong Bridge [17,18], Stonecutters bridge [19], Lysefjord Bridge [20], and Hardanger bridge [21]. However, several limitations inherent to field measurements require careful consideration. For instance, the measurements become feasible only after bridge construction, hindering their use in the design phase for optimizing aerodynamic performance. In addition, extensive instrumentation, specialized personnel, and prolonged monitoring periods contribute to significant costs and logistical challenges. Moreover, the measured data reflects the specific wind conditions and bridge characteristics at the site, limiting its generalizability to other locations or bridge geometries.

Machine learning (ML) techniques have recently emerged as increasingly popular tools in wind engineering applications [22], primarily due to their efficiency and accuracy. Complementary to existing methods, ML leverages various data sources, including wind tunnel tests, numerical simulations, and field measurements, to learn complex relationships between wind and bridge response. Once trained, these models can be utilized for a range of operational applications, from real-time monitoring and digital twin creation to risk simulations [23–30]. While ML applications in wind engineering are diverse, its use in bridge buffeting simulation remains limited. For example, Castellon et al. [31] employed Support Vector Regression (SVR) to predict the root mean square (RMS) value of buffeting response of the Hardanger bridge, demonstrating superior accuracy compared to Multilayer Perceptrons (MLPs). Zhang et al. [32] leveraged Quantile Random Forest with Bayesian optimization to predict the RMS of acceleration response of a long-span bridge under typhoon conditions, enabling uncertainty quantification. Laima et al. [33] proposed a dual-network approach to predict the power spectral density (PSD) and RMS of buffeting responses, achieving high accuracy. While recent applications of ML for bridge buffeting prediction show promise, significant challenges remain in capturing the full complexity of the phenomenon. The majority of studies have focused on estimating the RMS of the buffeting response or its behavior in the frequency domain. These approaches offer valuable insights, but they fail to provide the complete picture of the time-history response, which is crucial for comprehensive structural assessment and risk mitigation strategies. Li et al. [34] attempted to address this limitation by utilizing a Long Short-Term Memory (LSTM) network to simulate the time-history of buffeting response. However, their approach faced two key challenges: 1. The prediction was only applied to a few specific locations on the bridge, neglecting the potentially diverse response across the entire structure; and 2. The ML model suffered from error accumulation over time, resulting in decreased prediction accuracy and limiting the achievable prediction length. Therefore, it is important to address these challenges for unlocking the full potential of ML in bridge buffeting prediction.

This study proposes a novel hybrid machine learning (ML) framework to simulate the buffeting-induced response of long-span bridges over time, addressing key limitations in prior approaches. Unlike existing methods that primarily focus on root mean square (RMS) responses or frequency-domain analysis, this framework captures the complete time-history response across multiple degrees of freedom, offering a more comprehensive understanding of bridge dynamics under

buffeting excitation. Unlike previous studies, which typically focused on localized predictions, limited wind scenarios, and frequency-domain analysis, the proposed framework provides a comprehensive spatio-temporal response across multiple degrees of freedom under buffeting loads. The approach leverages the strengths of both autoencoders and LSTM networks to achieve efficient and accurate time-series prediction. The autoencoder networks first compress both wind speed and bridge displacement data into lower-dimensional latent spaces, capturing essential features and reducing computational burden. An LSTM network then leverages these compressed representations to model the temporal dependencies within the buffeting response, predicting the latent bridge response based on the encoded wind speed. Finally, the final predictive model employs both autoencoders and the trained LSTM: the first autoencoder encodes raw wind speed into the latent space, the LSTM predicts the latent bridge response from this encoding, and the second autoencoder reconstructs the final predicted bridge response vector. The proposed hybrid model's capabilities are evaluated on the Lysefjord Bridge through a case study. A simplified numerical model capturing the bridge's essential dynamic and aerodynamic characteristics is constructed to generate training and testing data. Wind speed time series are simulated using the Kaimal spectrum and Davenport coherence model for realistic wind conditions. The model's performance will be rigorously assessed via both interpolation and extrapolation tasks. A detailed analysis will be provided, highlighting the model's accuracy, limitations, and potential for real-world bridge response prediction under diverse wind conditions.

2. Buffeting analysis

2.1. Reference bridge model

The selected bridge's structural design draws inspiration from the Lysefjord Bridge in Norway. A simplified model is employed, focusing on capturing the critical dynamic and aerodynamic behaviors relevant to the specific bridge under study [20]. Table 1 presents the key structural and dynamic characteristics of this simplified model. The full specifications and details of the bridge model can be retrieved from Cheynet [35].

The bridge is idealized as a streamlined horizontal beam, with a coordinate system defined in Fig. 1. The modal shapes of the structure are extracted using the Galerkin method. The resulting modal shapes and natural frequencies have been compared to those obtained from a high-fidelity finite element model by Cheynet et al. [20]. The comparison demonstrates good overall agreement, suggesting that the simplified model effectively captures the bridge's global dynamic behavior. This model will subsequently serve as the platform for generating training and testing data for the proposed machine learning model.

2.2. Hazard analysis

Within the wind-fixed coordinate system, the wind vector is resolved into three orthogonal components: along-wind ($U = \bar{U} + u$), lateral-wind ($V = \bar{V} + v$), and vertical-wind ($W = \bar{W} + w$). Here, \bar{U} , \bar{V} and \bar{W} denote the mean wind components, while u , v and w represent the fluctuating components. Notably, for this study, \bar{V} and \bar{W} are assumed to

Table 1
Bridge structural parameters [35].

Property (unit)	Symbol	Value
Deck height (m)	D	2.76
Deck width (m)	B	12.3
Main span length (m)	L	446
Girder mass (kg/m)	m_g	5350
Main cables mass (kg/m)	m_c	408
Mass moment of inertia of the girder and cables (kg m ² /m)	I_0	82,430

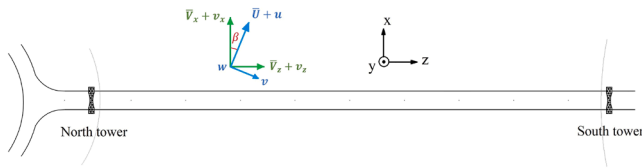


Fig. 1. Wind and bridge-based coordinate systems.

be zero, while \bar{U} holds a non-zero value. The corresponding wind components in the bridge-specific coordinate system are readily obtained by projecting the wind vector onto the bridge axes, leading to $V_x = \bar{V}_x + v_x$, $V_z = \bar{V}_z + v_z$, and $W = w$, as illustrated in Fig. 1.

This study employs a spectral approach to generate 26 wind speed time series, encompassing varying mean wind speeds from 5 m/s to 30 m/s with 1 m/s increments [36]. Each time series incorporates both mean and fluctuating wind components. The fluctuating components of the wind velocity were generated based on relevant turbulence statistics, including the power spectral density (PSD) and coherence function. The fluctuating wind components were obtained by applying the inverse Fourier Transform (IFT) to the chosen PSD while incorporating spatial coherence. The Davenport coherence function [1] modeled the spatial correlation of wind velocity fluctuations across the simulated domain. The Kaimal spectrum [37] served as the PSD model for generating individual wind components (u, v, w). This approach ensures realistic wind field representation with spatial and spectral characteristics mimicking the chosen turbulence models. The resulting time series spanned a total simulation time of 710 s with a sampling frequency of 18 Hz (period of 0.0556 s).

2.3. Buffeting analysis

The Lysefjord Bridge's dynamic response (lateral, vertical, and torsional) was evaluated in the time domain using generated turbulent wind velocity time series. A simplified model with three degrees of freedom (DOFs), for each cross section, representing lateral displacement (r_x), vertical displacement (r_y), and deck rotation (r_θ) was employed. A total of 40 nodes distributed along the bridge span ensured detailed structural representation. Both quasi-steady and strip theory methods were adopted to estimate the bridge response. Modal coupling between the three DOFs was considered to capture the full dynamic interaction. Notably, the quasi-steady theory was modified to incorporate aerodynamic damping, with the torsional motion specifically incorporating the expression $k_\theta B \dot{r}_\theta$, where k_θ represents the horizontal distance between the aerodynamic and shear center [20,35]. Fig. 2 depicts the bridge cross-section exposed to wind loads. In the wind coordinate system, these loads are: drag force F_D , lift force F_L and pitching moment F_M . The corresponding forces in the bridge coordinate system are: lateral force F_x , vertical force F_y and torsional moment $F_\theta = F_M$.

The dynamic response of the bridge deck is governed by the equation of motion:

$$M\ddot{r} + C\dot{r} + Kr = F \quad (1)$$

where M = mass matrix; C = damping matrix; K = stiffness matrix; F = total force vector acting on the deck; and $r = [r_x \ r_z \ r_\theta]^T$. The wind load, in its linearized form, can be expressed as [20,35]:

$$F = F_0[U] + F_1 \begin{bmatrix} v_x \\ w \end{bmatrix} - C_{ae} \begin{bmatrix} \dot{r}_x \\ \dot{r}_z \\ \dot{r}_\theta \end{bmatrix} - K_{ae} \begin{bmatrix} r_x \\ r_z \\ r_\theta \end{bmatrix} \quad (2)$$

where C_{ae} = aerodynamic damping; and K_{ae} = aerodynamic stiffness. All remaining components, including C_{ae} and K_{ae} , can be expressed as [20,35]:

$$F_0 = \frac{1}{2} \rho \bar{V}_x B \begin{bmatrix} D/BC_D \\ C_L \\ BC_M \end{bmatrix} \quad (3)$$

$$F_1 = \frac{1}{2} \rho \bar{V}_x B \begin{bmatrix} 2\frac{D}{B}C_D & \left(\frac{D}{B}C'_D - C_L\right) \\ 2C_L & \left(C_L + \frac{D}{B}C_D\right) \\ 2BC_M & BC'_M \end{bmatrix} \quad (4)$$

$$C_{ae} = \frac{1}{2} \rho \bar{V}_x B \begin{bmatrix} 2\frac{D}{B}C_D & \frac{D}{B}C'_D - C_L & k_\theta B \left(\frac{D}{B}C'_D - C_L\right) \\ 2C_L & C_L + \frac{D}{B}C_D & k_\theta B \left(C_L + \frac{D}{B}C_D\right) \\ 2BC_M & BC'_M & k_\theta B^2 C'_M \end{bmatrix} \quad (5)$$

$$K_{ae} = -\frac{1}{2} \rho \bar{V}_x^2 B \begin{bmatrix} 0 & 0 & \frac{D}{B}C'_D \\ 0 & 0 & C_L \\ 0 & 0 & BC'_M \end{bmatrix} \quad (6)$$

where C_D = drag coefficient; C_L = lift coefficient; and C_M = moment coefficient. A modal approach is adopted to compute the bridge's buffeting response. This method involves the determination of the structural response in the modal base [35]. The modal coupling between different modes is then incorporated to capture the full dynamic interaction. The Newmark method of time integration is employed to solve the equation of motion.

3. Proposed simulation framework

This study proposes a novel machine learning (ML) approach to simulate the buffeting-induced response of the selected bridge. The approach leverages two key components: 1. Dimensionality reduction where both the input (wind speed) and output (bridge displacement = $[r_x \ r_y \ r_\theta]$) data are compressed using separate autoencoders; 2. Time series simulation with Long Short-Term Memory (LSTM) Network to capture the temporal dependencies present in the buffeting response time series. The compressed input data from the autoencoders is fed into the LSTM, enabling it to learn and predict the bridge displacements [38]. By utilizing autoencoders to reduce the dimensionality of both the input wind speed and output bridge displacement data, the learning process for the LSTM is simplified [38]. This allows the LSTM to focus on capturing the most relevant temporal dependencies, leading to more accurate and efficient predictions. Additionally, autoencoders help filter out noise and irrelevant information, improving the model's robustness. This hybrid approach overcomes the limitations of using LSTMs alone, especially when dealing with high-dimensional and noisy data, making it well-suited for modeling complex, real-world phenomena like bridge buffeting. The detailed architecture of the proposed model will be presented after a brief summary of each component.

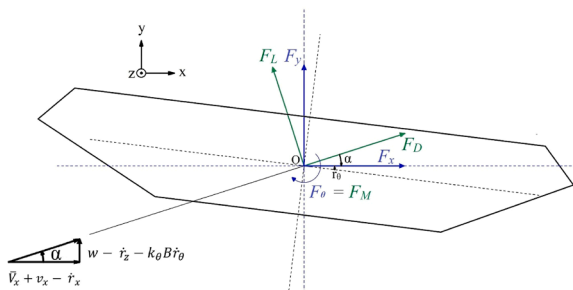


Fig. 2. Cross-section of the bridge subjected to the wind load.

3.1. Autoencoder neural networks

Autoencoders are a type of neural network architecture employed for unsupervised learning tasks. They excel at compressing high-dimensional data into a lower-dimensional latent space while preserving essential features. This capability is particularly valuable when dealing with extensive spatial dimensions in both input and output data. The autoencoder architecture comprises two key functions: An encoder (φ) which maps the input data (x) into a reduced-dimensional latent representation (z) such that $z = \varphi(x)$; and a decoder ψ which reconstructs the original input data from the latent representation ($\hat{x} = \psi(z)$). The training process aims to minimize the reconstruction error between the original input (x) and the reconstructed output (\hat{x}). This forces the autoencoder to learn a compressed representation (z) that captures the salient features of the input data. Compared to linear dimensionality reduction techniques like Principal Component Analysis (PCA), autoencoders can handle complex non-linear relationships within the data, leading to more effective representation learning [39, 40], especially for tasks like bridge buffeting response modeling.

This study highlights the important role of dimensionality reduction due to the inherent high dimensionality of both inputs and outputs associated with the large-scale bridge structure. Dividing the bridge span into 40 nodes leads to an expansive input dimension when multiplied by the number of wind components. Similarly, the number of bridge response DOFs defines the output dimension, resulting in both input and output spaces being highly multi-dimensional. Consequently, employing a single neural network directly on such high-dimensional data becomes computationally intractable. By leveraging dimensionality reduction techniques, a lower-dimensional subspace is identified, also known as the latent space, capturing the essential information of the original data. This facilitates the implementation of reduced-order models based on the low-dimensional representation, enabling efficient analysis and prediction of the bridge response while overcoming the limitations imposed by high dimensionality. Fig. 3 presents a schematic diagram illustrating the architecture of a standard autoencoder model.

3.2. LSTM networks

Long Short-Term Memory (LSTM) networks belong to a class of recurrent neural networks (RNNs) renowned for their ability in capturing long-range dependencies within sequential data. This characteristic positions them uniquely for sequence prediction tasks, making them highly prevalent in applications like machine translation, speech recognition, and time series analysis. Conventional RNNs are hampered by the vanishing/exploding gradient problem, rendering them ineffective in learning long-term dependencies. In contrast, LSTMs circumvent this limitation by employing a sophisticated gating mechanism that selectively retains relevant information across extended temporal stretches. This ability to effectively manage long-range dependencies

significantly empowers LSTMs in sequence-to-sequence modeling compared to traditional RNNs. Fig. 4 visualizes the typical architecture of an LSTM network, incorporating multiple hidden layers composed of both LSTM units and fully connected layers, sandwiched between the input and output layers.

Within the temporal domain ($\tau = 1, 2, \dots, t$), the LSTM network establishes a pairwise mapping between input sequences and their corresponding output sequences. Each LSTM layer is comprised of a collection of memory cells characterized by their weight parameters and bias terms. These cells utilize a sophisticated gating mechanism consisting of an internal cell state, input gate, output gate, and forget gate. This combined system empowers selective information retention, forgetting, and update through time, rendering LSTMs adept at capturing long-range dependencies in sequential data.

3.3. Proposed model

This study proposes a hybrid machine learning model to efficiently capture the complex relationship between bridge wind speed components and corresponding buffeting-induced responses. The true function f representing this relationship maps an input vector of wind speed components $\mathbf{X} \in \mathbb{R}^n$ to an output vector of bridge responses $\mathbf{Y} \in \mathbb{R}^m$, where n and m denote the dimensions of the input and output spaces, respectively, such that:

$$f(\mathbf{X}) = \mathbf{Y} \quad (7)$$

Directly modeling f can be challenging due to the high dimensionality of \mathbf{X} and \mathbf{Y} . Therefore, the proposed approach introduces two latent spaces, namely the input latent space ($\mathbf{z}_{in} \in \mathbb{R}^p$) and the output latent space ($\mathbf{z}_{out} \in \mathbb{R}^q$), with reduced dimensions p and q compared to n and m . An autoencoder architecture is employed to learn low-dimensional representations of the input and output data. The encoder components φ_{in} and φ_{out} map the original input \mathbf{X} and output \mathbf{Y} to their corresponding latent vectors \mathbf{z}_{in} ($\mathbf{z}_{in} = \varphi_{in}(\mathbf{X})$) and \mathbf{z}_{out} ($\mathbf{z}_{out} = \varphi_{out}(\mathbf{Y})$), respectively. Subsequently, an LSTM model g is trained to predict the output latent space \mathbf{z}_{out} from the input latent space \mathbf{z}_{in} (i.e., $g(\mathbf{z}_{in}) = \hat{\mathbf{z}}_{out}$). This LSTM model captures the temporal dynamics of the bridge response under varying wind conditions. Finally, a decoder component ψ_{out} reconstructs the original output space \mathbf{Y} from the predicted latent output $\hat{\mathbf{z}}_{out}$. The overall architecture of the proposed hybrid model, including the autoencoder components, the LSTM model, and the decoder, is presented in Fig. 5.

Following training, the final predictive model, as illustrated in Fig. 5, leverages components from both autoencoders and the LSTM network: 1. encoder (φ_{in}) from the first autoencoder which maps the raw wind speed data (\mathbf{X}) to the low-dimensional latent space; 2. LSTM network which predicts the latent bridge response ($\hat{\mathbf{z}}_{out}$) based on the input latent representation from φ_{in} ; and 3. decoder (ψ_{out}) from the second autoencoder which reconstructs the final predicted bridge response vector ($\mathbf{r} = [r_x \ r_y \ r_\theta]$) from the predicted latent output ($\hat{\mathbf{z}}_{out}$). The hybrid model effectively predicts the structural response of bridges under wind excitation by combining the dimensionality reduction capabilities of autoencoders with the temporal forecasting abilities of the LSTM network. The resulting predictive model offers a compact and computationally efficient tool for real-time monitoring and assessment of bridge health under diverse wind conditions.

4. Results and discussion

4.1. Data preparation

A total of 26 wind speed time series were generated for training and testing the proposed hybrid machine learning model. These time series cover a range of mean wind speeds from 5 m/s to 30 m/s, with an increment of 1 m/s. The fluctuating wind components (u, v, w) were

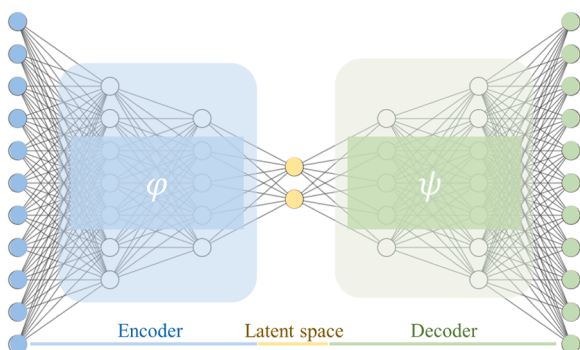


Fig. 3. Architecture of typical autoencoders.

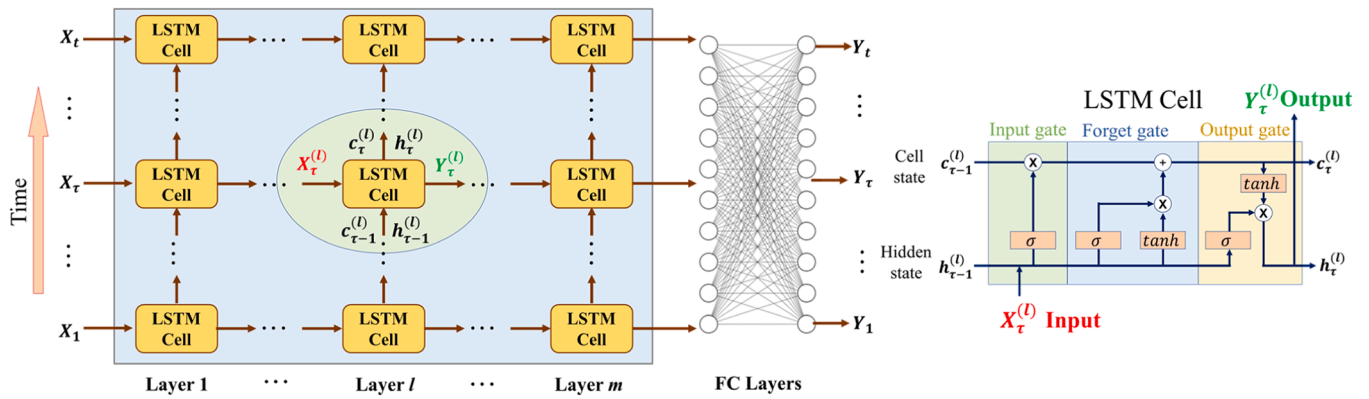


Fig. 4. Architecture of a standard LSTM network (left) and an LSTM cell (right).

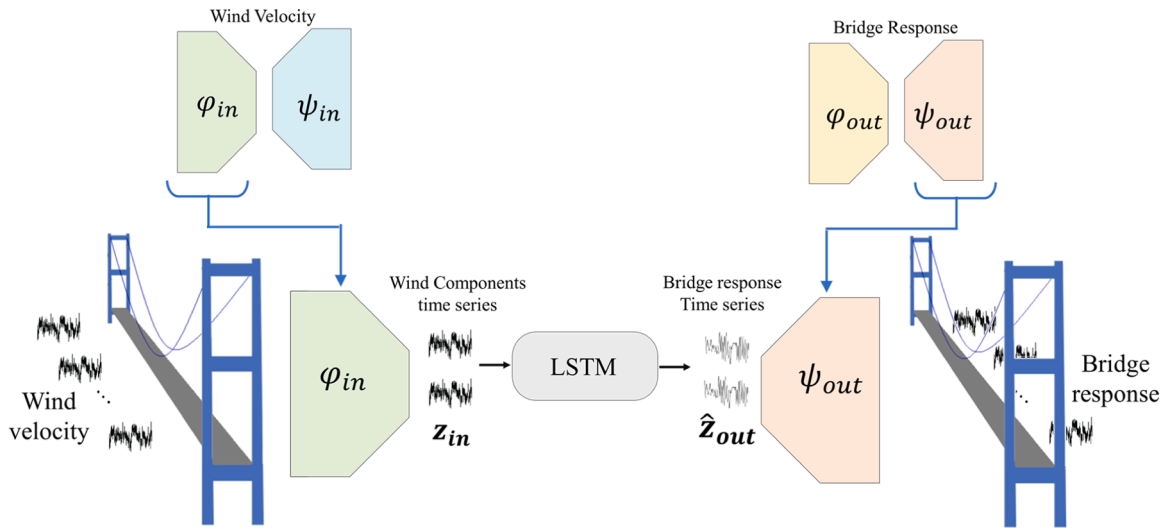


Fig. 5. Architecture of the proposed hybrid model.

generated using the methodology described in Sect. 2.2, which combines the Kaimal spectrum with the Davenport coherence model. The Kaimal model requires the friction velocity (u_*), which is calculated using the logarithmic mean wind profile as:

$$u_* = \kappa * \bar{U} / \log\left(\frac{z_{ref}}{z_0}\right) \quad (8)$$

where $\kappa = 0.4$ the von Karman constant; $z_{ref} = 55m$ reference height of the bridge deck; and $z_0 = 0.05m$ roughness height. The Davenport coherence model utilizes the following empirical decay coefficients $C_u^z = 7$, $C_v^u = 10$, $C_v^v = 7$, $C_w^v = 10$, $C_w^z = 6.5$, and $C_w^w = 3$ [35]. These coefficients influence the spatial correlation between wind speed components at different locations on the bridge, ensuring realistic wind field representation. Each generated time series encompasses a total simulation time of 710 s, discretized with a sampling period of 0.0556 seconds. Fig. 6 presents an example of bridge response at mid-span, in terms of $r = [r_x \ r_y \ r_\theta]$. The mean wind speed in this example is $\bar{U} = 9m/s$. As Fig. 6 demonstrates, the along-wind response r_x exhibits consistently positive values. In contrast, the vertical r_y and torsional response r_θ fluctuate around zero, reflecting their inherently dynamic nature under wind excitation.

The generated time series data was divided into training and testing sets to evaluate the proposed hybrid machine learning model. A subset of 6 time series, carefully chosen to represent diverse wind conditions within the anticipated operational range (7, 14, 17, 24, 26, and 29 m/s),

was allocated for training. This selection ensures the model can handle scenarios within its intended domain. The remaining 20 time series, encompassing wind speeds ranging from 5 to 30 m/s, constitute the testing set, allowing assessment of both extrapolation capabilities beyond the training range (below 7 m/s and above 29 m/s) and interpolation within the range. Each time series consists of wind speed components (inputs) and bridge response vectors (outputs) recorded at 40 nodes along the bridge span. Due to fixed boundary conditions at the ends, only 38 internal nodes with non-zero response were retained for analysis. Furthermore, considering the negligible influence of the lateral wind component (v) on the overall bridge response, only the along-wind (U) and vertical wind (w) components were utilized as model inputs. This choice leads to 76 input nodes for the first autoencoder (processing wind speed components). The second autoencoder, processing bridge response, has 114 input nodes corresponding to the three degrees of freedom ($r_x \ r_y \ r_\theta$) measured at each of the 38 retained nodes.

4.2. Model training

The initial step in constructing the hybrid model involves training two independent autoencoders: one for the wind speed components and another for the bridge response. Each autoencoder aims to learn low-dimensional representations of the respective input data by minimizing a loss function that penalizes deviations from the original input during reconstruction. The commonly employed autoencoder loss function, as expressed in Eq. (9), utilizes the L_2 norm (denoted by $\|\cdot\|_2^2$)

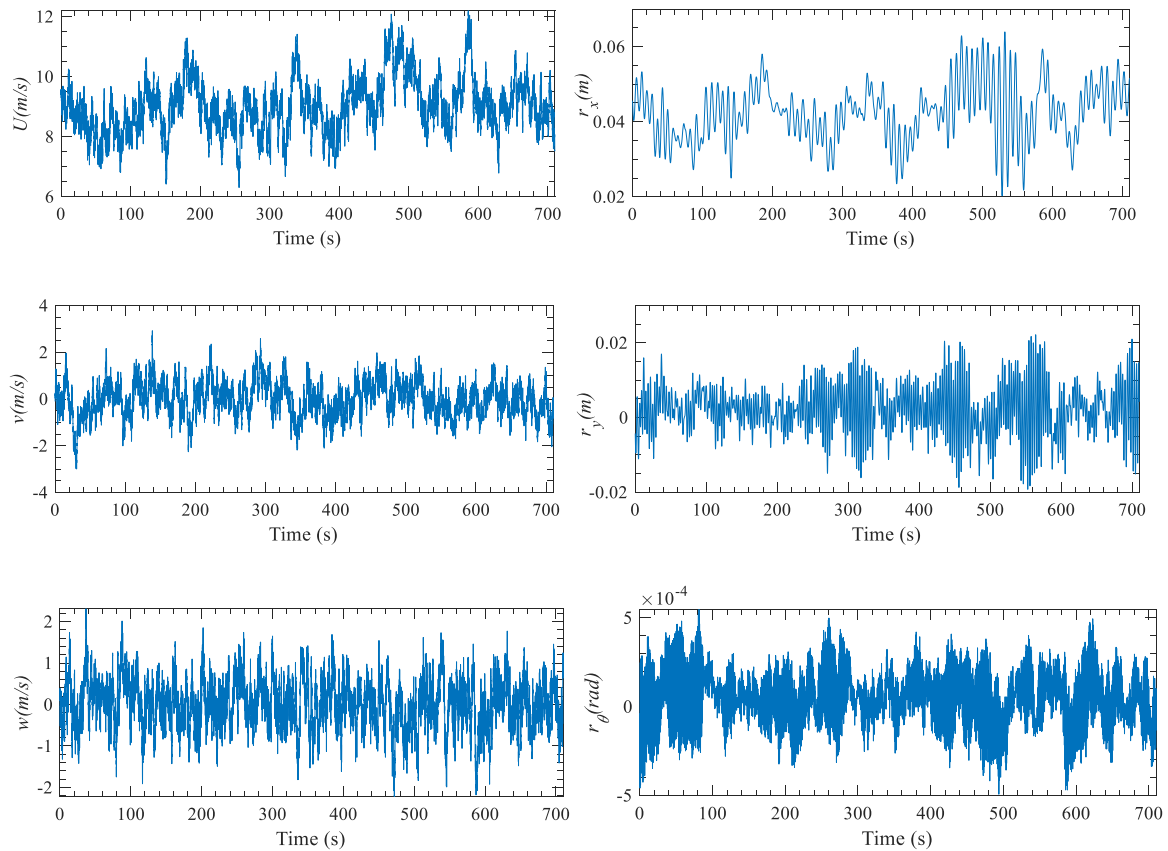


Fig. 6. Time series of the wind speed (left) for the case scenario of $\bar{U} = 9\text{m/s}$ and the corresponding bridge response (right).

to measure the reconstruction error:

$$\mathcal{L}_{AE} = \|X - \psi(\varphi(X))\|_2^2 \quad (9)$$

where \mathcal{L}_{AE} = autoencoder loss; and X = input data to the autoencoder (either wind speed components or bridge response). Effective training of both autoencoders necessitates careful selection of various hyperparameters, such as the network architecture, activation function, learning rate and network size. These hyperparameters significantly influence the autoencoders' learning capability and ultimately, the quality of extracted features. While advanced optimization techniques like Bayesian optimization exist, this study employed a trial-and-error approach for hyperparameter tuning. Extensive evaluation revealed superior performance from separate autoencoders for the along-wind (U) and vertical wind (w) components. Each wind autoencoder employs a 38–24–12–3–12–24–38 architecture. Similarly, individual autoencoders were trained for each of the three bridge response components (r_x , r_y , r_θ). Each response autoencoder adopts a 38–24–12–2–12–24–38 architecture. For all autoencoders, the Adam optimization algorithm [41] was employed due to its efficient handling of sparse gradients and high-dimensional parameters. The $Tanh$ activation function was selected for all layers except the bottleneck layer, which serves as the latent space representation. A learning rate of 0.0001 was selected based on empirical testing to ensure proper convergence and training stability. All input data (wind components and bridge responses) were normalized between 0 and 1. This normalization facilitates faster convergence and avoids biases towards features with larger initial scales. The performance of the trained autoencoder models was evaluated using quantitative metrics, summarized in Table 2. For clarity, AE_1^U and AE_2^w denote the autoencoder models trained on the along-wind (U) and vertical wind (w) components, respectively. The AE_3^x , AE_4^y , and AE_5^θ represent the autoencoder models trained on the

Table 2

Performance of the training and testing for the autoencoders.

Performance (MSE)	Input		Output		
	AE_1^U	AE_2^w	AE_3^x	AE_4^y	AE_5^θ
Training	6.3e-03	4.7e-03	2.06e-04	1.79e-04	3.80e-04
Testing	8.4e-03	5.3e-03	6.33e-04	2.63e-04	5.88e-04

three bridge response components, r_x , r_y and r_θ , respectively.

As evident from Table 2, the Mean Squared Error (MSE) values for all models are relatively low, indicating satisfactory performance that justifies their use in the subsequent step of the hybrid model. Following autoencoder training, the low-dimensional latent space representations produced by AE_1^U (along-wind) and AE_2^w (vertical wind) are concatenated, resulting in a 6-dimensional input vector for the LSTM model. Similarly, the combined latent space dimensions from AE_3^x , AE_4^y , and AE_5^θ generate a 6-dimensional output vector for the LSTM. The LSTM architecture comprises a single cell with a 25-dimensional hidden state vector and a $Tanh$ activation function. A dense layer with a linear activation function is subsequently added after the LSTM cell as the output layer. All training data were normalized between -1 and 1 . The training process utilizes truncated backpropagation through time (BPTT) as proposed by Simpson et al. [36]. Fig. 7 presents the training curve of the LSTM network, showcasing a decreasing loss function over training epochs. The final loss value (MSE) after convergence is $1.32\text{e-}06$.

To mitigate overfitting and underfitting, several strategies were employed during the model training. First, autoencoders were utilized to compress high-dimensional wind and response data into lower-dimensional latent spaces, enabling the model to focus on the most relevant features while reducing noise and less significant variations. This dimensionality reduction simplified the input and output spaces

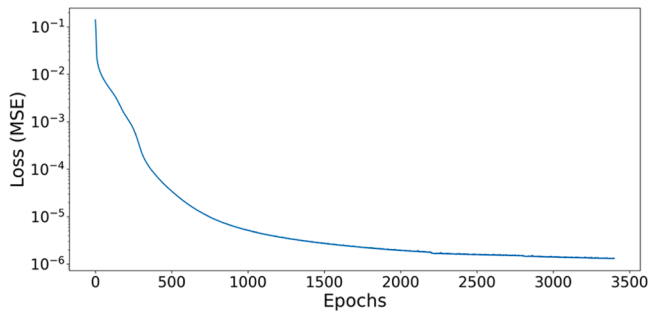


Fig. 7. Performance of the training process of the LSTM network.

and prevented the model from keeping irrelevant details in the training data. Regularization techniques, such as dropout layers, were applied to the LSTM network to reduce reliance on specific neurons, encouraging the learning of generalized patterns. Moreover, early stopping was implemented to monitor and halt training when performance ceased to improve, minimizing the risk of overfitting. Validation was performed on both interpolation and extrapolation tasks to ensure generalization across a range of wind scenarios, including conditions beyond the training data. Additionally, extensive hyperparameter tuning optimized the model parameters such as the number of layers, neurons, and learning rate, achieving a balance between model complexity and prediction accuracy while avoiding overfitting and underfitting. The training dataset incorporated diverse wind scenarios spanning various intensities and conditions, promoting generalization and reducing overfitting by exposing the model to a broad spectrum of buffeting responses. These strategies collectively enabled the model to accurately capture the complexities of buffeting response while avoiding overfitting and underfitting.

4.3. Application

Following successful training of the individual components, the hybrid model is assembled as depicted in Fig. 8. This combined architecture leverages the dimensionality reduction benefits of autoencoders to efficiently handle complex input data and the LSTM network’s ability to learn and predict the temporal evolution of the bridge response.

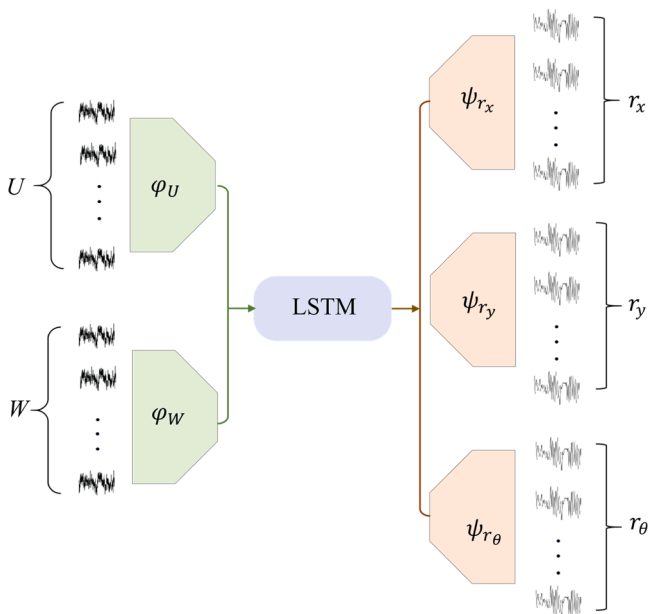


Fig. 8. Architecture of the predictive hybrid model.

Specifically, the hybrid model consists of two input encoders φ_U and φ_W followed by an LSTM network, then three output decoders ψ_{r_x} , ψ_{r_y} and ψ_{r_θ} as illustrated by Fig. 8.

As depicted in Fig. 8, the hybrid model leverages both autoencoders and the LSTM network for bridge response prediction. The process can be described in three key steps: 1. The first set of encoders, φ_U and φ_W process the wind speed time series data. Each encoder performs dimensionality reduction, mapping the high-dimensional wind speed components (U and w) to separate lower-dimensional latent representations; 2. The concatenated latent representations from φ_U and φ_W are fed into the LSTM network. This network, due to its inherent capability in handling temporal sequences, analyzes the dynamic relationship between wind speed variations and the resulting bridge response. By learning from historical data, the LSTM is able to capture the evolving temporal patterns within the wind and their impact on the bridge structure; 3. The final stage involves three decoders, ψ_{r_x} , ψ_{r_y} and ψ_{r_θ} . Each decoder receives the predicted latent representation of the bridge response from the LSTM network and maps it back to the original high-dimensional space. This reconstruction provides the predictions for the along-wind (r_x), vertical (r_y), and torsional (r_θ) components of the bridge response.

The hybrid model demonstrated strong performance on the independent test set, achieving a low root mean squared error (RMSE) of 0.085 across the entire bridge, as calculated from the normalized output values. This result highlights the good generalization capability of the proposed hybrid model. To further investigate the model’s performance, specific scenarios are selected from the test set. Fig. 9 showcases the predicted bridge response for a moderate wind speed of 21 m/s. The predicted response, represented by the vector $[r_x \ r_y \ r_\theta]$, is visualized at two key locations: the mid-span and a point near one-third of the span. Additionally, a zoomed-in plot highlights the time-series response at these locations, allowing for a closer examination of temporal dynamics.

Fig. 9 demonstrates the hybrid model’s effectiveness in replicating bridge response time series due to buffeting. Quantitative assessment confirms this, with RMSE values at the mid-span location being 0.047 m, 0.026 m, and 3.4e-04 rad for r_x , r_y and r_θ , respectively. Similar results are observed near the third of the span, with RMSE values of 0.037 m, 0.029 m, and 2.6e-04 rad for r_x , r_y and r_θ , respectively. Additionally, visual inspection of PSDs suggests the model captures the signal’s frequency content well, indicating successful training. These findings demonstrate the model’s capability to accurately predict the bridge response under buffeting conditions. It should be noted that there are some discrepancies in r_x , which was anticipated due to its unique temporal and spectral characteristics compared to r_y and r_θ . To enhance the simulation results for r_x , an alternative approach will be presented in Sect. 4.4.

Fig. 10 investigates the hybrid model’s ability to extrapolate beyond the training data range. Two scenarios are chosen: Scenario 1 represented by a weak intensity with a mean wind speed of 6 m/s (below training range); and Scenario 2 represented by a high intensity with a mean wind speed of 30 m/s (above training range). Due to their potential impact on bridge stability, only the vertical (r_y) and rotational (r_θ) bridge responses are visualized in Fig. 10.

Fig. 10 demonstrates good agreement between the bridge response predicted by the hybrid model and the corresponding responses obtained through finite element simulations. Specifically, for the $\bar{U} = 6\text{m/s}$ scenario, the obtained RMSE values are 0.053 m and 2.6e-04 rad for r_y and r_θ , respectively. Additionally, for the $\bar{U} = 30\text{m/s}$ scenario, the RMSE values are 0.021 m and 2.9e-04 rad for r_y and r_θ , respectively. This observation, particularly for scenarios beyond the training data range, highlights the robustness and generalizability of the hybrid model for predicting the bridge response under unseen wind conditions.

To investigate the time-dependent prediction error, Table 3 summarizes the Mean Absolute Error (MAE) values at five different time

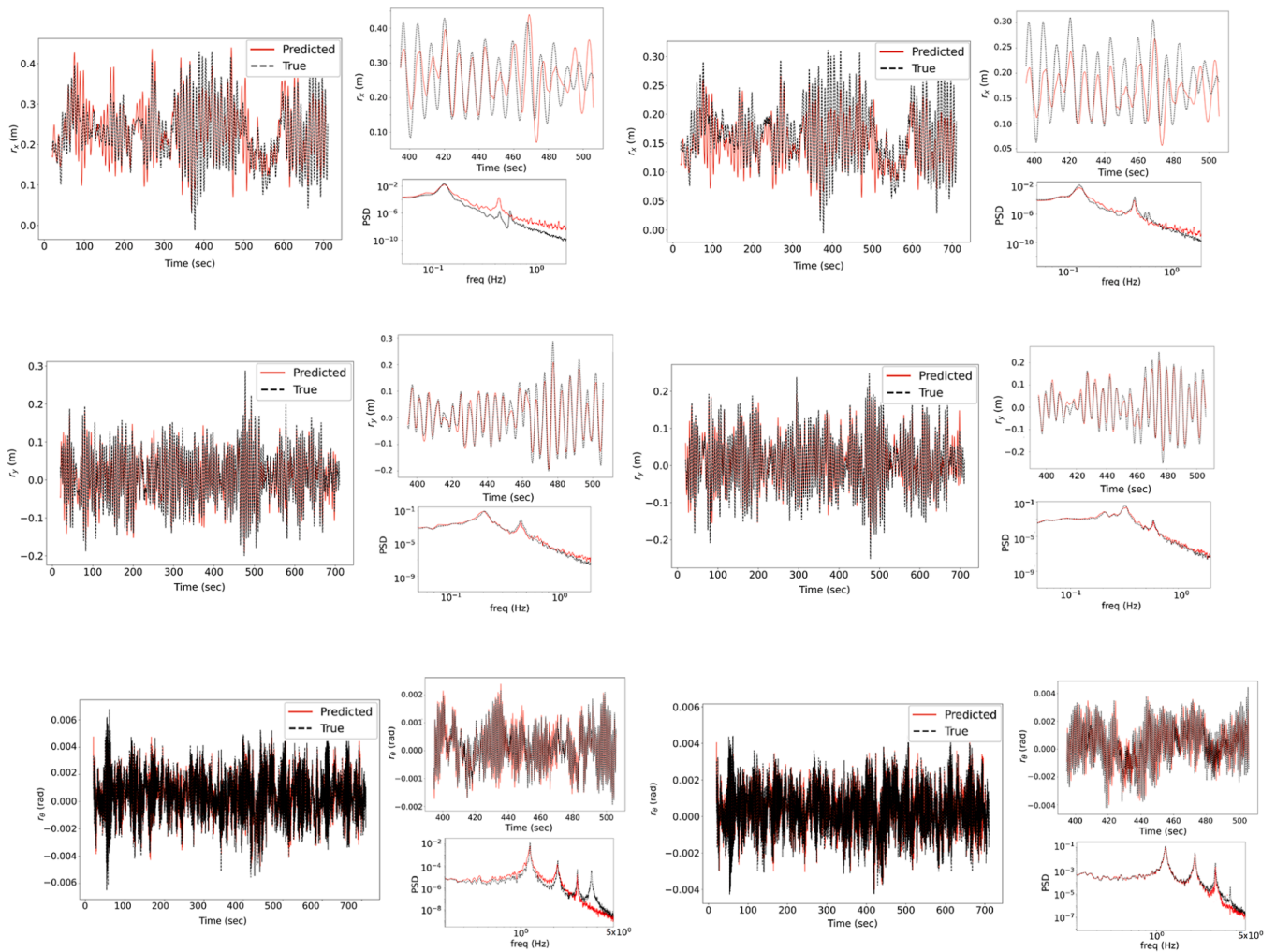


Fig. 9. Time-series bridge response and PSD at midspan (left column) and third of the span (right column) for a 21 m/s mean wind speed.

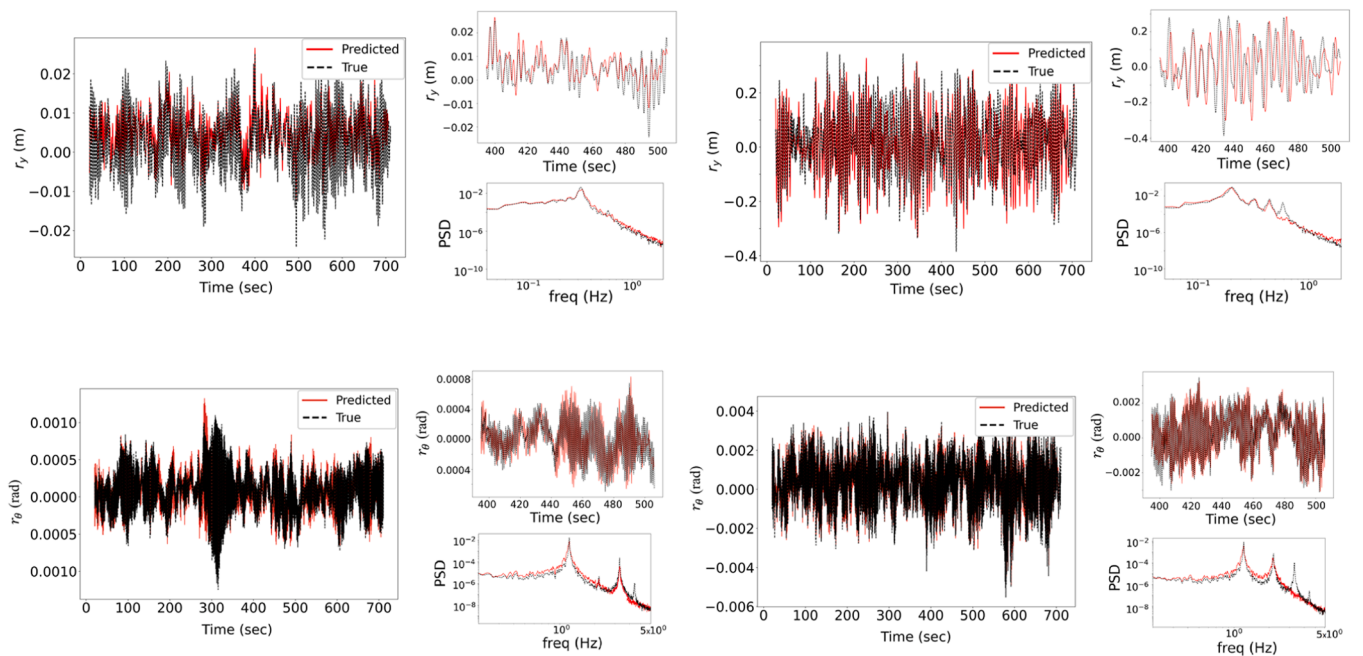


Fig. 10. Time-series bridge response and PSD at midspan for $\bar{U} = 6m/s$ (left column), and $\bar{U} = 30m/s$ (right column).

Table 3
Mean absolute error of predicted response components at different time steps for two wind scenarios for all DOFs across the bridge.

		$t(s)$	32.6	111.0	278.6	528.4	667.2
Scenario 1	$r_x(m)$		7.6e-02	3.1e-02	4.5e-02	3.1e-02	4.1e-02
	$r_y(m)$		2.5e-02	2.7e-02	2.1e-02	1.9e-02	2.4e-02
	$r_\theta(rad)$		3.3e-02	0.9e-02	1.1e-02	0.6e-02	3.0e-02
Scenario 2	$r_x(m)$		7.1e-02	3.4e-02	8.9e-02	3.9e-02	2.4e-02
	$r_y(m)$		2.9e-02	1.3e-02	1.8e-02	0.6e-02	1.7e-02
	$r_\theta(rad)$		1.5e-02	1.9e-02	2.0e-02	3.6e-02	0.9e-02

steps for two wind scenarios ($\bar{U} = 9$ m/s and $\bar{U} = 27$ m/s) for all nodes across the bridge. The results indicate that the prediction errors remain consistently low, particularly at larger time steps. For instance, the maximum MAE values for r_x , r_y and r_θ are 8.9e-02 m, 2.9e-02 m, and 3.3e-02 rad, respectively. Notably, the absence of error accumulation demonstrates the model's stability and its ability to maintain accurate predictions over extended time periods.

4.4. Discussion

Long-span bridges are susceptible to buffeting which significantly impacts the fatigue life of structural components and can synergistically interact with other wind loads, potentially leading to major structural deficiencies [24]. Therefore, accurate assessment of buffeting is critical for ensuring long-term bridge serviceability. Traditional methods to simulate the buffeting-induced response can be computationally expensive, limiting their applications in areas like real-time risk prediction, probabilistic risk assessment, and digital twin integration [32]. This study proposes a novel hybrid machine learning model for efficient and accurate simulation of the 3D displacement response (r_x , r_y and r_θ) of long-span bridges under buffeting excitation. The model combines autoencoder networks for dimensionality reduction of both the input wind components and the 3D displacement outputs. This compression step facilitates efficient processing and reduces model complexity. Subsequently, an LSTM network learns the complex non-linear relationship between the low-dimensional wind representation and the corresponding bridge displacement representation. This approach leverages the strengths of autoencoders in handling high-dimensional data and the capability of LSTMs in capturing temporal dependencies present in wind turbulence and bridge response.

Dimensionality reduction via autoencoders serves as a crucial preprocessing step for the subsequent LSTM network, the central component of the hybrid architecture. The autoencoders' effectiveness in uncovering informative latent spaces directly impacts the overall model performance. Inaccurate latent representations compromise the LSTM's ability to learn the complex temporal dynamics between wind components and bridge response, potentially leading to suboptimal predictions. This study employs separate autoencoders for both input wind components (U and w) and bridge response outputs (r_x , r_y , and r_θ). While a combined input-output autoencoder architecture is feasible, separate encoders were chosen to enhance training and testing performance based on distinct time-frequency characteristics of the data. For instance, the temporal and spectral signatures of r_x differ significantly from r_y , and r_θ , posing challenges in finding an optimal latent space within a single autoencoder. Leveraging this non-linear dimensionality reduction technique, the input wind components are compressed from 76 to 6 features and the bridge response outputs from 114 to 6 features. This substantial reduction in both input and output dimensions significantly improves the robustness of the subsequent LSTM model training. High-dimensional data can exacerbate computational costs and overfitting in LSTM training. By effectively capturing critical information in lower-dimensional spaces, the model achieves better training and testing performance compared to scenarios with uncompressed data.

Despite achieving satisfactory performance during training and

testing as evidenced by overall model metrics, discrepancies remain, particularly evident for the r_x response (Fig. 9). This was anticipated due to the distinct temporal and spectral characteristics of r_x compared to r_y and r_θ . To further enhance the simulation accuracy, an alternative approach utilizing a separate LSTM model dedicated solely to r_x prediction was explored. Fig. 11 presents the results of this dedicated r_x prediction model for a moderate wind speed of 21 m/s at two different locations (midspan and the third of the span), demonstrating improved performance for this specific response component.

The RMSE values for r_x prediction by the dedicated LSTM model are 9.85e-03 m and 8.31e-03 m for the midspan and third of the span, respectively. These results represent a significant improvement compared to the combined LSTM model, which achieved RMSE values of 0.047 m and 0.037 m for the same locations. Notably, the dedicated model achieved 79.1 % and 77.5 % reductions in RMSE for the midspan and third of the span, respectively, demonstrating its effectiveness in capturing the unique dynamics of r_x compared to the combined approach.

The generalizability of ML-based models is a critical consideration. While the proposed hybrid framework combining autoencoders and LSTM has the potential for broader application, its predictive accuracy is inherently tied to the quality and specificity of the training data. To ensure accurate predictions for other long-span bridges, the model should be retrained with data capturing their unique geometric, aerodynamic, and dynamic properties. However, transfer learning techniques can potentially accelerate the training process for bridges with similar characteristics. This study focuses on the Lysefjord Bridge, demonstrating the model's capability to accurately predict buffeting responses for a wide range of wind scenarios, significantly outperforming traditional numerical simulations in terms of computational efficiency. This rapid prediction capability has significant potential for real-time monitoring, digital twin integration, and structural optimization. The model's strong interpolation and extrapolation performance within the Lysefjord Bridge's aerodynamic and dynamic range underscores its robustness. While retraining with bridge-specific data is necessary for other structures to ensure accuracy, the methodology presented in this study offers a powerful and efficient foundation for modeling buffeting responses across various long-span bridges. This research underscores the potential of ML-based approaches to advance bridge aerodynamics and structural response prediction.

While this study used a trial-and-error approach for identifying suitable hyperparameters, adopting advanced optimization techniques such as Bayesian optimization could further improve model performance. Bayesian optimization automates the hyperparameter search, enabling efficient identification of optimal settings compared to manual methods. Additionally, the training and testing datasets were generated using a simplified buffeting model. This approach neglected unsteady effects in the buffeting response calculations, which could potentially impact the simulation results. To enhance the dataset's accuracy, more advanced data generation techniques could be employed. These could incorporate recent theoretical findings, CFD simulations, wind tunnel experiments (e.g., for unit-step or unit-impulse response functions), or field measurement data. This would help ensure that the model is trained and evaluated on data that closely mirrors real-world bridge behavior under wind loading. Incorporating physics-informed learning into the model framework could also be beneficial, as it would enable the integration of governing physical equations directly into the model. By embedding scientifically valid principles, the model's predictions could be further constrained, potentially resulting in more robust and generalizable simulations [42–44]. Expanding the methodology to include a wider range of bridge configurations would also enhance its applicability and generalizability. This could involve training and testing on data from different bridge types to ensure the model's ability to predict buffeting responses across diverse structural designs. Moreover, the current framework focuses on predicting buffeting responses and does not account for other aerodynamic forces, such as

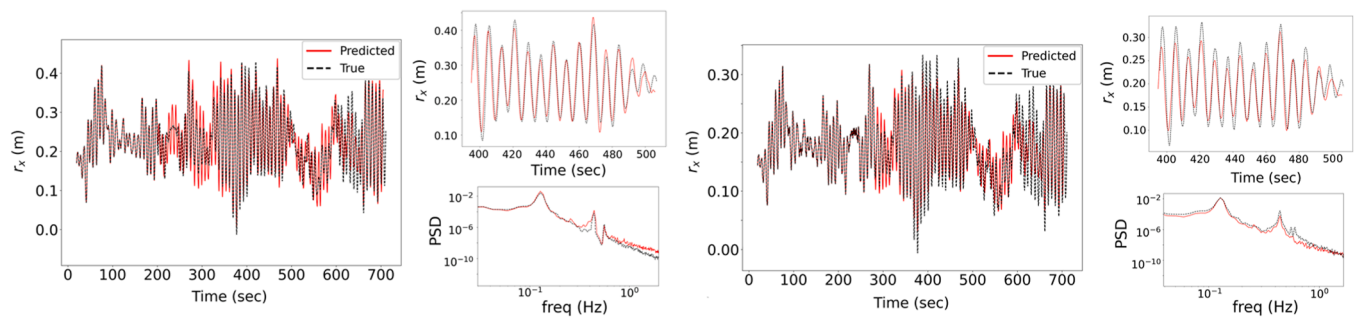


Fig. 11. Time-series bridge response and PSD at midspan (left column) and third of the span (right column) for $\bar{U} = 21\text{m/s}$.

motion-induced forces or vortex-induced vibrations. Considering these effects in future work would be beneficial for modeling the full range of wind-induced responses. Finally, while this study used vanilla autoencoders for dimensionality reduction, this approach may be suboptimal for handling large and complex datasets. Convolutional autoencoders (CAEs) offer enhanced spatial feature extraction, reduced computational load through parameter sharing, and improved generalization by capturing localized features in high-dimensional data. CAEs can help reduce the risk of overfitting and increase model robustness and reliability, especially under real-world conditions that may introduce noise.

5. Conclusion

This study presented a novel hybrid machine learning framework for real-time prediction of buffeting-induced responses in long-span bridges. This framework, combining autoencoders and Long Short-Term Memory (LSTM) networks, achieved efficient and accurate time-series prediction. Autoencoders effectively compressed high-dimensional data while retaining key features, leading to reduced computational demands. The LSTM network utilized these compressed representations to capture temporal dependencies, enabling accurate response prediction based on encoded wind speed. The final model seamlessly integrated both autoencoders and the trained LSTM. The evaluation on a simplified model of the Lysefjord Bridge demonstrated good simulation accuracy across both training and testing sets. Specifically, the model achieved a low RMSE values of 0.085 across the entire bridge, on the testing set, suggesting good over all performance. This showcases the proposed framework's potential as a compact and computationally efficient tool for real-time bridge health monitoring and assessment under diverse wind conditions, paving the way for proactive measures to ensure safety and serviceability.

CRedit authorship contribution statement

Mohajeri Nav Foad: Writing – review & editing, Writing – original draft, Visualization, Validation, Software, Methodology, Investigation, Formal analysis, Data curation, Conceptualization. **Snaiki Reda:** Writing – review & editing, Writing – original draft, Supervision, Software, Resources, Methodology, Investigation, Funding acquisition, Formal analysis, Data curation, Conceptualization.

Declaration of Competing Interest

The authors declare that they have no known competing financial interests or personal relationships that could have appeared to influence the work reported in this paper.

Acknowledgements

This work was supported by the Natural Sciences and Engineering Research Council of Canada (NSERC) [grant number CRSNG RGPIN

2022-03492].

References

- [1] Davenport AG. Buffeting of a suspension bridge by storm winds. *J Struct Div* 1962; 88(3):233–70.
- [2] Chen X, Kareem A. New frontiers in aerodynamic tailoring of long span bridges: an advanced analysis framework. *J Wind Eng Ind Aerodyn* 2003;91(12-15):1511–28.
- [3] Zhu LD, Xu YL. Buffeting response of long-span cable-supported bridges under skew winds. Part 1: theory. *J Sound Vib* 2005;281(3-5):647–73.
- [4] Diana G, Resta F, Rocchi D. A new numerical approach to reproduce bridge aerodynamic non-linearities in time domain. *J Wind Eng Ind Aerodyn* 2008;96(10-11):1871–84.
- [5] Hu L, Xu YL, Zhu Q, Guo A, Kareem A. Tropical storm-induced buffeting response of long-span bridges: enhanced nonstationary buffeting force model. *J Struct Eng* 2017;143(6):04017027.
- [6] Allard L, Snaiki R. Buffeting-Induced fatigue damage assessment of a long-span bridge under a changing climate scenario. *Journal of Bridge Engineering* 2025;30(3):04024118.
- [7] Miyata T, Yamata H, Yokoyama K, Kanazaki T, Iijima T. Construction of boundary layer wind tunnel for long-span bridges. *J Wind Eng Ind Aerodyn* 1992;42(1-3): 885–96.
- [8] Diana G, Rocchi D, Belloli M. Wind tunnel: a fundamental tool for long-span bridge design. In: Design, assessment, monitoring and maintenance of bridges and infrastructure networks. Routledge; 2020. p. 121–43.
- [9] He X, Zou S. Advances in wind tunnel experimental investigations of train-bridge systems. *Tunn Undergr Space Technol* 2021;118:104157.
- [10] Kildal O, Li L, Hearst RJ, Petersen ØW, Øiseth O. On the use of an active turbulence grid in wind tunnel testing of bridge decks. *J Wind Eng Ind Aerodyn* 2023;233: 105331.
- [11] Kim BC, Yhim SS. Buffeting analysis of a cable-stayed bridge using three-dimensional computational fluid dynamics. *J Bridge Eng* 2014;19(11):04014044.
- [12] Blocken B. 50 years of computational wind engineering: past, present and future. *J Wind Eng Ind Aerodyn* 2014;129:69–102.
- [13] Löhner R, Haug E, Michalski A, Muhammad B, Drego A, Nanjundiah R, Zarfam R. Recent advances in computational wind engineering and fluid-structure interaction. *J Wind Eng Ind Aerodyn* 2015;144:14–23.
- [14] Kim S, Jung H, Kong MJ, Lee DK, An YK. In-situ data-driven buffeting response analysis of a cable-stayed bridge. *Sensors* 2019;19(14):3048.
- [15] Xu YL, Zhu LD. Buffeting response of long-span cable-supported bridges under skew winds. Part 2: case study. *J Sound Vib* 2005;281(3-5):675–97.
- [16] Wang H, Li A, Guo T, Xie J. Field measurement on wind characteristic and buffeting response of the Runyang Suspension Bridge during typhoon Matsa. *Sci China Ser E Technol Sci* 2009;52(5):1354–62.
- [17] Wang H, Li A, Niu J, Zong Z, Li J. Long-term monitoring of wind characteristics at Sutong Bridge site. *J Wind Eng Ind Aerodyn* 2013;115:39–47.
- [18] Mao JX, Wang H, Feng DM, Tao TY, Zheng WZ. Investigation of dynamic properties of long-span cable-stayed bridges based on one-year monitoring data under normal operating condition. *Struct Control Health Monit* 2018;25(5):e2146.
- [19] Hu L, Xu YL, Huang WF. Typhoon-induced non-stationary buffeting response of long-span bridges in complex terrain. *Eng Struct* 2013;57:406–15.
- [20] Cheynet E, Jakobsen JB, Snæbjörnsson J. Buffeting response of a suspension bridge in complex terrain. *Eng Struct* 2016;128:474–87.
- [21] Fenerci A, Øiseth O, Rønquist A. Long-term monitoring of wind field characteristics and dynamic response of a long-span suspension bridge in complex terrain. *Eng Struct* 2017;147:269–84.
- [22] Wu T, Snaiki R. Applications of machine learning to wind engineering. *Front Built Environ* 2022;8:811460.
- [23] Fang C, Tang H, Li Y. Stochastic response assessment of cross-sea bridges under correlated wind and waves via machine learning. *J Bridge Eng* 2020;25(6): 04020025.
- [24] Liu P, Zhao L, Fang G, Ge Y. Explicit polynomial regression models of wind characteristics and structural effects on a long-span bridge utilizing onsite monitoring data. *Struct Control Health Monit* 2021;28(5):e2705.

- [25] Lystad TM, Fenerci A, Øiseth O. Full long-term extreme buffeting response calculations using sequential Gaussian process surrogate modeling. *Eng Struct* 2023;292:116495.
- [26] Bernardini E, Spence SM, Wei D, Kareem A. Aerodynamic shape optimization of civil structures: a CFD-enabled Kriging-based approach. *J Wind Eng Ind Aerodyn* 2015;144:154–64.
- [27] Wu T, Kareem A. Modeling hysteretic nonlinear behavior of bridge aerodynamics via cellular automata nested neural network. *J Wind Eng Ind Aerodyn* 2011;99(4): 378–88.
- [28] Li S, Laima S, Li H. Data-driven modeling of vortex-induced vibration of a long-span suspension bridge using decision tree learning and support vector regression. *J Wind Eng Ind Aerodyn* 2018;172:196–211.
- [29] Nieto F, Montoya MC, Hernández S, Kusano I, Casteleiro A, Álvarez AJ, Jurado JÁ, Fontán A. Aerodynamic and aeroelastic responses of short gap twin-box decks: box geometry and gap distance dependent surrogate based design. *J Wind Eng Ind Aerodyn* 2020;201:104147.
- [30] Montoya MC, Nieto F, Hernández S, Kusano I, Álvarez AJ, Jurado JÁ. CFD-based aeroelastic characterization of streamlined bridge deck cross-sections subject to shape modifications using surrogate models. *J Wind Eng Ind Aerodyn* 2018;177: 405–28.
- [31] Castellon DF, Fenerci A, Øiseth O. A comparative study of wind-induced dynamic response models of long-span bridges using artificial neural networks, support vector regression and buffeting theory. *J Wind Eng Ind Aerodyn* 2021;209:104484.
- [32] Zhang YM, Wang H, Mao JX, Xu ZD, Zhang YF. Probabilistic framework with bayesian optimization for predicting typhoon-induced dynamic responses of a long-span bridge. *J Struct Eng* 2021;147(1):04020297.
- [33] Laima S, Feng H, Li H, Jin Y, Han F, Xu W. A Buffeting-Net for buffeting response prediction of full-scale bridges. *Eng Struct* 2023;275:115289.
- [34] Li S, Li S, Laima S, Li H. Data-driven modeling of bridge buffeting in the time domain using long short-term memory network based on structural health monitoring. *Struct Control Health Monit* 2021;28(8):e2772.
- [35] Cheynet, E., 2016. Wind-induced vibrations of a suspension bridge: A case study in full-scale. University of Stavanger, PhD thesis UiS, no. 326.
- [36] Simpson T, Dervilis N, Couturier P, Maljaars N, Chatzi E. Reduced order modeling of non-linear monopile dynamics via an AE-LSTM scheme. *Front Energy Res* 2023; 11:1128201.
- [37] Kaimal JC, Wyngaard JG, Izumi Y, Coté OR. Spectral characteristics of surface-layer turbulence. *Q J R Meteorol Soc* 1972;98(417):563–89.
- [38] Simpson T, Dervilis N, Chatzi E. Machine learning approach to model order reduction of nonlinear systems via autoencoder and LSTM networks. *Journal of Engineering Mechanics* 2021;147(10):04021061.
- [39] Naeini SS, Snaiki. A novel hybrid machine learning model for rapid assessment of wave and storm surge responses over an extended coastal region. *Coastal Engineering* 2024;190:104503.
- [40] Naeini, S.S., Snaiki, R. and Wu, T., 2024. Advancing Spatio-temporal Storm Surge Prediction with Hierarchical Deep Neural Networks. *arXiv preprint arXiv: 2410.12823*.
- [41] Kingma, D.P. and Ba, J., 2015. Adam: a method for stochastic optimization. In: *Proceedings of the third international conference for learning representations, San Diego*.
- [42] Snaiki R, Wu T. Knowledge-enhanced deep learning for simulation of tropical cyclone boundary-layer winds. *J Wind Eng Ind Aerodyn* 2019;194:103983.
- [43] Snaiki R, Wu T. Knowledge-enhanced deep learning for simulation of extratropical cyclone wind risk. *Atmosphere* 2022;13(5):757.
- [44] Li S, Snaiki R, Wu T. A knowledge-enhanced deep reinforcement learning-based shape optimizer for aerodynamic mitigation of wind-sensitive structures. *Comput-Aided Civ Infrastruct Eng* 2021;36(6):733–46.